Crystal Structures of the Carboxyl Terminal Domain of Rat 10-Formyltetrahydrofolate Dehydrogenase: Implications for the Catalytic Mechanism of Aldehyde Dehydrogenases†

Yaroslav Tsybovsky, Henry Donato, Natalia I. Krupenko, Christopher Davies,* and Sergey A. Krupenko*

Department of Biochemistry and Molecular Biology, Medical University of South Carolina, Charleston, South Carolina 29425

Received September 20, 2006; Revised Manuscript Received January 3, 2007

ABSTRACT: 10-Formyltetrahydrofolate dehydrogenase (FDH) catalyzes an $NADP^+$-dependent dehydrogenase reaction resulting in conversion of 10-formyltetrahydrofolate to tetrahydrofolate and CO_2. This reaction is a result of the concerted action of two catalytic domains of FDH, the amino-terminal hydrolase domain and the carboxyl-terminal aldehyde dehydrogenase domain. In addition to participation in the overall FDH mechanism, the C-terminal domain is capable of $NADP^+$-dependent oxidation of short chain aldehydes to their corresponding acids. We have determined the crystal structure of the C-terminal domain of FDH and its complexes with oxidized and reduced forms of NADP. Compared to other members of the ALDH family, FDH demonstrates a new mode of binding of the 2′-phosphate group of NADP via a water-mediated contact with Gln600 that may contribute to the specificity of the enzyme for NADP over NAD. The structures also suggest how Glu673 can act as a general base in both acylation and deacylation steps of the reaction. In the apo structure, the general base Glu673 is positioned optimally for proton abstraction from the sulfur atom of Cys707. Upon binding of $NADP^+$, the side chain of Glu673 is displaced from the active site by the nicotinamide ring and contacts a chain of highly ordered water molecules that may represent a pathway for translocation of the abstracted proton from Glu673 to the solvent. When reduced, the nicotinamide ring of NADP is displaced from the active site, restoring the contact between Cys707 and Glu673 and allowing the latter to activate the hydrolytic water molecule in deacylation.

10-Formyltetrahydrofolate dehydrogenase (FDH,[1] EC 1.5.1.6) catalyzes $NADP^+$-dependent conversion of 10-formyltetrahydrofolate (10-fTHF) to tetrahydrofolate (THF) and CO_2 (*1*), a reaction that appears to be important in the pathway for *de novo* purine biosynthesis (*2*, *3*). While FDH is abundant in several tissues, its levels are ubiquitously low in tumors (*2*) and expression of the enzyme in FDH-deficient cancer cells strongly suppresses proliferation and induces apoptosis (*2*, *4*). It is therefore likely that cancer cells down-regulate FDH to support a higher rate of *de novo* purine biosynthesis. Other functions proposed for FDH include removal of excess one-carbon groups from the folate pool (*5*); storage of cellular folates as THF (*6*, *7*); and participation in formate oxidation (*8*, *9*). Recent studies have also implicated FDH in the regulation of cellular methylation reactions in human neuroblastoma cells (*10*).

The reaction catalyzed by FDH is a combination of two unrelated reactions, executed by the functional domains of the protein: a hydrolase reaction that occurs in the N-terminal domain and an aldehyde dehydrogenase (ALDH) reaction that resides in the C-terminal domain. When expressed individually, each domain is capable of independent catalysis (*11*−*13*). Our previous studies suggest that the 10-fTHF dehydrogenase reaction is composed of three steps: (i) hydrolysis of the folate substrate and release of the formyl group; (ii) transfer of the formyl from the hydrolase domain to the aldehyde dehydrogenase domain; and (iii) oxidation of this group to CO_2 (*14*−*16*). The role of the intermediate domain that separates the N-terminal and C-terminal domains remains unclear, but it may act to transfer the formyl between the two active centers.

The C-terminal domain of FDH shares up to 50% sequence identity with members of the ALDH family of enzymes (*11*). Functionally, aldehyde dehydrogenases are a very diverse group of enzymes and can oxidize a large variety of aldehydes including glyceraldehyde 3-phosphate, short-chain aldehydes, retinaldehyde, and environmental aromatic xenobiotics (*17*). The carboxyl-terminal domain of FDH possesses ALDH activity toward short-chain aldehydes (*12*), and, by its sequence and substrate specificity, this domain

† This work was supported by a grant from the National Institutes of Health (DK54388 to S.A.K.) and by an NSF/EPSCoR grant (EPS-0132573). Supporting institutions may be found at www.ser-cat.org/members.html. Use of the Advanced Photon Source was supported by the U.S. Department of Energy, Office of Science, Office of Basic Energy Sciences, under Contract No. W-31-109-Eng-38.

* To whom correspondence should be addressed: Sergey A. Krupenko, Department of Biochemistry and Molecular Biology, Medical University of South Carolina, 173 Ashley Ave., Charleston, SC 29425; tel, 843 792-0845; fax, 843 792-8565; e-mail, krupenko@musc.edu. Christopher Davies, Department of Biochemistry and Molecular Biology, Medical University of South Carolina, 173 Ashley Ave., Charleston, SC 29425; tel, 843 792-1468; fax, 843 792-8568; e-mail, davies@musc.edu.

[1] Abbreviations: ALDH, aldehyde dehydrogenase; FDH, 10-formyltetrahydrofolate dehydrogenase; GAPDH, glyceraldehyde-3-phosphate dehydrogenase; GAPN, nonphosphorylating glyceraldehyde 3-phosphate dehydrogenase; ADH, alcohol dehydrogenase; rmsd, root mean square deviation.

10.1021/bi0619573 CCC: $37.00
Published on Web 02/16/2007

of FDH is most similar to class 1 and class 2 ALDHs. Mammalian class 1 and class 2 ALDHs are tetrameric cytosolic or mitochondrial enzymes with variable substrate specificities, but all manifest a strong preference for NAD as a coenzyme (*17*). The ALDH domain of FDH is also organized as a tetramer (*12*, *18*), and the full-length enzyme is cytosolic (*1*). In contrast with the class 1 and class 2 enzymes, however, FDH utilizes NADP, with specificity for NAD being 1000-fold lower (*12*).

The postulated mechanism of ALDH catalysis comprises two steps, acylation and deacylation, with a covalent intermediate (*19*−*21*). Crystal structures of ALDHs have revealed the close proximity of the two catalytic residues, cysteine 302 and glutamate 268 (in class 1 and 2 enzymes) within the active site (*22*−*25*). In acylation, Glu268 is postulated to be the general base that abstracts a proton from Cys302, activating the latter for nucleophilic attack on the carbonyl carbon of the substrate (*23*, *25*, *26*). Although, in coenzyme-bound structures of ALDH enzymes, the side chain of Glu268 is too far away to deprotonate the sulfhydryl group of Cys302 directly (*23*, *25*), it has been proposed that either (i) a water molecule positioned between the two catalytic residues can help in abstracting a proton or (ii) repositioning of the two residues during catalysis brings them closer to each other (*23*). Others, however, have argued against a role for Glu268 in acylation. Specifically, a downward shift in the pK_a attributed to the cysteine nucleophile in nonphosphorylating glyceraldehyde 3-phosphate dehydrogenase (GAPN) from 8.5 to 6.1, which was observed upon binding coenzyme, was taken as evidence that Glu268 is not required for acylation (*27*). By contrast, it is generally accepted that Glu268 acts as a general base in deacylation by activating a water molecule during hydrolysis of the thioester bond (*23*, *26*−*28*). Assuming a dual role in acylation and deacylation, it remains unclear, however, how the deprotonated form of Glu is regenerated prior to deacylation.

Crystal structures have also revealed highly variable binding of the nicotinamide portion of the coenzyme (*22*−*24*, *28*, *29*). While in several structures this part of the coenzyme is disordered (*24*, *30*, *31*), two distinct conformations of the coenzyme, each with a well-ordered nicotinamide ring, have also been observed (*25*, *28*, *32*). In the so-called hydride transfer (or extended) conformation, the nicotinamide ring lies in close proximity to the active site cysteine (*23*, *25*), whereas in the hydrolysis (or contracted) conformation, the nicotinamide ring has moved away from the active site allowing a water molecule to access the thioester carbon of the acyl-enzyme intermediate (*28*, *32*).

Here, we report the crystal structure of the ALDH domain of FDH, including its two complexes with oxidized and reduced NADP. Curiously, the complex with $NADP^+$ appears to show a covalent bond between the cysteine nucleophile (Cys707) and C4 of the nicotinamide ring whose existence is also supported by mutational and spectroscopic studies. We interpret these structures to propose a mechanism of ALDH catalysis that invokes a direct role for Glu268 in both acylation and deacylation and suggests a proton relay mechanism for regeneration of the basic form of Glu673 after acylation.

EXPERIMENTAL PROCEDURES

Vector Construction. To generate the construct for expression of the ALDH domain of FDH, the fragment of cDNA corresponding to amino acid residues 1−397 was deleted from the pRSET vector containing cDNA for full-length FDH, inserted through the *Eco*RI site (*33*). For this purpose, two unique restriction sites, *Sna*BI and *Hpa*I, were introduced, the first immediately downstream of the sequence encoding for the His tag, and the second upstream of the sequence encoding for amino acid 398. This was achieved by site-directed mutagenesis using the QuikChange kit (Stratagene) and the following primers:

5′-CATCATCATCATACGTATGGCTAGCATG-3′ and

5′-CATGCTAGCCATACGTATGATGATGATG-3′ (*Sna*BI site)

and

5′-CCTAGTGAGGAAGTTAACAGGGGAGG ACGAC-3′ and

5′-GTCGTCCTCCCCTGTTAACTTCCTCACTAGG-3′ (*Hpa*I site)

The sequence between the two restriction sites was excised with *Sna*BI/*Hpa*I endonucleases, and the plasmid was religated through blunt ends. The resulting expression vector encoded residues 398−902 of full-length FDH and included a His_5 tag at the N-terminus with flanking spacers (ArgGlySer and ThrThrGly) (Figure 1A). This protein construct is called C_t-FDH, and the amino acid sequence is numbered according to full-length FDH.

Protein Expression and Purification. C_t-FDH was expressed in *Escherichia coli* using the same procedures developed for the N-terminal domain of FDH (*33*) except that, to increase the yield of the soluble recombinant protein, expression was performed at 22 °C. The protein was purified from the soluble cell fraction in a single step using Ni-NTA chromatography (GE-Healthcare).

Site-Directed Mutagenesis. C707S and E673A mutants of C_t-FDH were produced using the QuikChange site-directed mutagenesis kit (Stratagene). These were confirmed by DNA sequencing, and the mutant proteins were expressed and purified as described for C_t-FDH. The correct folding of the mutants was confirmed by circular dichroism spectroscopy (E673A) and X-ray crystallography (C707S) (data not shown).

Assay of ALDH Activity. The ALDH activity of the E673A mutant of C_t-FDH was measured by following the increase in absorbance at 340 nm as a result of formation of NADPH. The standard assay contained 0.22 μM E673A mutant, 100 μM $NADP^+$, and 10 mM propanal in 0.1 M Tris, pH 8.4. The reaction was initiated by the addition of propanal. All measurements were done at 25 °C using Shimadzu 2401PC double beam spectrophotometer.

Crystallization and Data Collection. Prior to crystallization trials, the protein was concentrated to 8 mg/mL in 20 mM Tris-HCl, pH 8.1, using Amicon microconcentrators (Millipore). Dithiothreitol and NaN_3 were added to the protein samples to final concentrations of 6 mM and 0.02% (w/v), respectively.

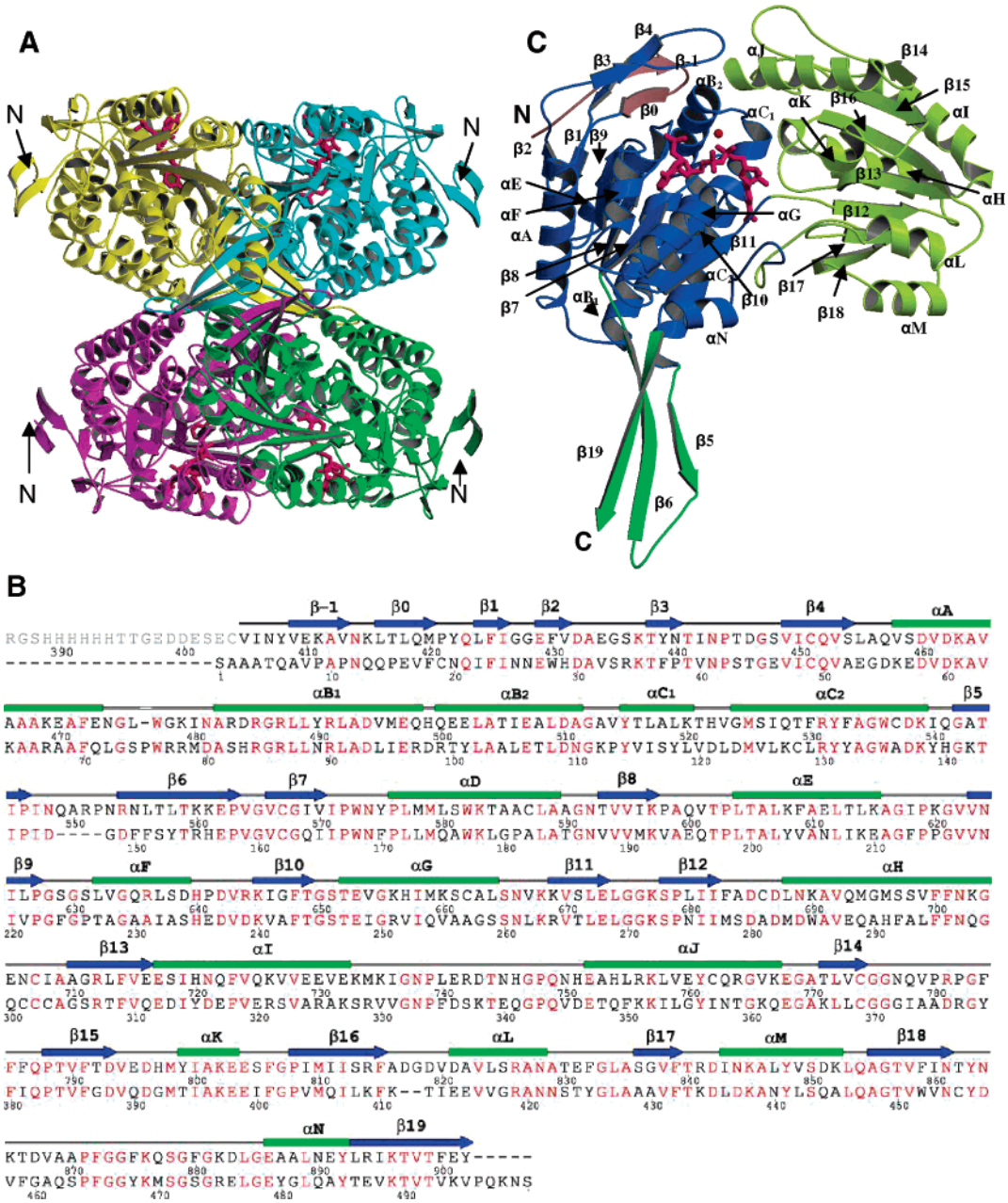

FIGURE 1: The crystal structure of C_t-FDH. (A) Ribbon diagram of the C_t-FDH tetramer in which the four subunits are colored differently. $NADP^+$ molecules are represented in stick form and colored red. The N-terminal residues (Val405) are denoted as N. (B) Sequence alignment of C_t-FDH (upper sequence) vs human mitochondrial ALDH (lower sequence). The secondary structure elements of C_t-FDH are shown as arrows (β-strands) and bars (α-helices). (C) Ribbon representation of one subunit of C_t-FDH in which the NADP-binding domain is colored blue, the catalytic domain is yellow, and the oligomerization domain is green. The strands β-1 and β0 are colored light pink. The secondary structure elements are labeled. An $NADP^+$ molecule with a Mg^{2+} atom (red sphere) is shown bound to the NADP-binding domain. The figure was prepared using MOLSCRIPT (*64*), Raster3D (*65*) (A, C), and SecSeq (xray.imsb.au.dk/∼deb/secseq) (B).

Crystals in the absence of coenzyme were grown by the vapor diffusion technique in hanging drops over wells containing 1.4−1.5 M ammonium sulfate and 0.1 M Tris-HCl, pH 7.0−7.5. These appeared after 3 to 7 days incubation at 15 °C and reached maximal size in two weeks. Crystals of $NADP^+$-bound C_t-FDH were obtained by overnight soaking crystals of the native enzyme in mother liquor containing 5−10 mM $NADP^+$ and 10 mM $MgCl_2$. Crystals of the NADPH-bound complex were obtained by overnight soaking in mother liquor containing 10 mM NADPH. Prior to data collection, all crystals were passed through mother liquor containing 22−25% glycerol and then flash-frozen *in situ* at 100 K using an X-Stream Cryostream (Rigaku MSC).

An initial data set extending to 2.8 Å resolution was collected from an $NADP^+$-bound crystal of C_t-FDH on an RAXIS IV^{++} image plate detector mounted on a RU-H3R rotating anode X-ray generator operating at 50 kV and 100 mA. The crystals belong to space group $P2_1$ with cell dimensions $a = 259.5$ Å, $b = 194.4$ Å, $c = 97.3$ Å, and $\beta = 108.9°$. There is one tetramer per asymmetric unit (*34*). Subsequent data sets were collected at a wavelength of 1.0 Å on a MAR300 CCD detector (MAR-USA) at the SER-CAT beamline ID22 at the Advanced Photon Source (APS, Argonne National Laboratory, Argonne, IL). These data were processed using HKL2000 (*35*), and the statistics are shown in Table 1.

Table 1: Data Collection and Refinement Statistics[a]

	native	$NADP^+$ complex	NADPH complex
resolution (Å)	50.0−1.7 (1.76−1.70)	50.0−2.0 (2.07−2.00)	50.0−2.15[b] (2.23−2.15)
completeness %	97.5 (95.8)	97.3 (85.3)	99.2 (98.4)
mean $I/\sigma I$	10.1 (2.5)	5.8 (1.7)	12.4 (3.7)
redundancy	5.1 (4.8)	4.8 (3.1)	5.4 (5.1)
R_{merge} (%)	8.5(55.8)	13.6 (55.2)	9.9 (50.6)
no. of water molecules	1795	1848	786
R_{cryst} (%)	17.4	16.9	18.1
R_{free} (%)	18.8	19.0	20.2
rmsd bond lengths (Å)	0.011	0.012	0.013
rmsd bond angles (°)	1.26	1.29	1.38
Ramachandran plot:			
% residues in			
most favored regions	91.1	90.3	90.6
additionally allowed regions	8.5	9.3	9.0
generously allowed regions	0.2	0.2	0.2
disallowed regions	0.2	0.2	0.2

[a] The figures in parentheses refer to the highest resolution shell of the data. [b] This structure was refined at 2.2 Å resolution.

Model Building and Refinement. The 2.8 Å data collected from the crystal of the $NADP^+$-bound enzyme were used to solve the structure by molecular replacement using MOLREP (*36*). The search model used was the structure of retinal dehydrogenase II from *Rattus norvegicus* (*24*) (PDB entry 1BI9), which shares 49.4% sequence identity with C_t-FDH. The initial model was refined by CNS (*37*) and thereafter by alternating rounds of REFMAC5 (*38*) and manual revision using O (*39*). $NADP^+$ molecules were identified by examination of the $|F_O| - |F_C|$ and $2|F_O| - |F_C|$ electron density maps. The structures of native C_t-FDH, the NADPH-bound complex, and the final structure of the $NADP^+$-bound complex were obtained by refinement of the initial $NADP^+$-bound structure against the respective synchrotron data using REFMAC5. Based on minimizing peaks of positive and negative density in the $|F_O| - |F_C|$ difference density maps, the coenzyme molecules were assigned an occupancy of 0.9 in all structures. Similarly, the side chain of Glu673, one of the residues involved in the catalytic reaction, was assigned an occupancy of 0.6−0.8, depending on the subunit. Solvent molecules were introduced using ARP/wARP (*40*) and inspected manually. During all steps of the refinement, 5% of the data were reserved to calculate the free *R*-factor and this assignment was maintained for all data sets. The refinement statistics are shown in Table 1.

For all three structures, the final models contain residues 405−902; the N-terminal histidine tag and residues 398−404 cannot be seen due to apparent conformational flexibility. The models possess good stereochemistry, as defined by PROCHECK (*41*) (Table 1). The only residue found in the disallowed region of the Ramachandran plot is Leu884, which is located inside the hydrophobic core of the protein and exhibits well-defined electron density. Coordinates and structure factors have been deposited in the Protein Data Bank with codes 2O2P, 2O2Q, and 2O2R for the native structure, the binary complex with $NADP^+$, and the binary complex with NADPH, respectively.

RESULTS

Structure of the Apoenzyme. The structure of C_t-FDH in the absence of coenzyme was determined at 1.7 Å resolution. The protein comprises four identical subunits related by noncrystallographic 222 point group symmetry and is arranged as a dimer of dimers (Figure 1A) (*23*, *28*, *29*). All the subunits maintain the same general structure, although the positions of some side chains vary among individual subunits. The overall structure of C_t-FDH shares the general fold of ALDH of class 1 and 2 (*23*, *28*). The subunit comprises three domains (Figure 1C): an N-terminal NADP-binding domain (residues 405−539, 564−675, and 867−893), a catalytic domain (residues 676−885), and an oligomerization domain (residues 540−563 and 894−902). The NADP-binding and catalytic domains are α/β in structure, whereas the oligomerization domain contains a three-stranded antiparallel β-sheet.

The structure can be superimposed onto that of sheep liver ALDH (PDB code 1BXS) (*28*) and human mitochondrial ALDH (PDB code 1O00) (*32*) with rmsd between 474 C_α atoms of 0.98 Å and 1.36 Å, respectively (Figure 2B), which is somewhat higher than the typical values obtained within the ALDH1 and 2 families (*28*). Compared to other ALDH enzymes, the highest divergence in structure occurs at the N-terminal region of the molecule (Figure 2A). While in most ALDH enzymes the first 7 to 20 amino-terminal residues are either not seen in the structure because of conformational disorder or adopt irregular loop structure, residues 409−413 and 416−420 of C_t-FDH form two antiparallel β-strands, denoted as β-1 and β0 (Figure 1B), which pack against αB_2 and αE (Figure 2A). These regions differ because, in full-length FDH, the intermediate domain precedes the C-terminal domain whereas other ALDH enzymes comprise only the ALDH domain. After Gln423, the main chain of C_t-FDH closely follows that of ALDH1 and ALDH2.

The location of the N termini of C_t-FDH suggests that the intermediate domain and, before that, the N-terminal hydrolase domain are located at the vertices of the tetramer (Figure 1A). This arrangement, however, does not resolve the question of whether there is a direct interaction between the hydrolase and the ALDH domains of FDH, via intra-subunit or intersubunit interactions. The apparent positioning of the hydrolase domain beyond the tetramer, though, is consistent with the monomeric state of this domain when expressed separately (*13*).

Active Site. The active site of C_t-FDH is situated at the bottom of an approximately 12 Å deep substrate entrance tunnel located between the coenzyme-binding and the catalytic domains of the protein. The amino acid composition of the tunnel is closer to that of ALDH1, which is known to be more specific toward larger substrates than most ALDH2 members (*24*, *28*). The general arrangement of residues within the active site itself is similar to that observed in the ALDH family, including the cysteine nucleophile, Cys707 (*23*, *28*) (Figure 3A). The only amino acid difference in the active site occurs at position 706, where C_t-FDH has an asparagine instead of a conserved cysteine present in structures of ALDH1 and 2.

Interestingly, when the C_t-FDH structures were refined with a single conformation for the side chain of Cys707, a peak of negative electron density was observed consistently in the $|F_O| - |F_C|$ difference map at the current position of the sulfur atom, as well as a positive peak situated at a distance of 1.8 Å from the C_β atom of the cysteine. Hence, an alternative conformation of the S_γ atom was modeled and

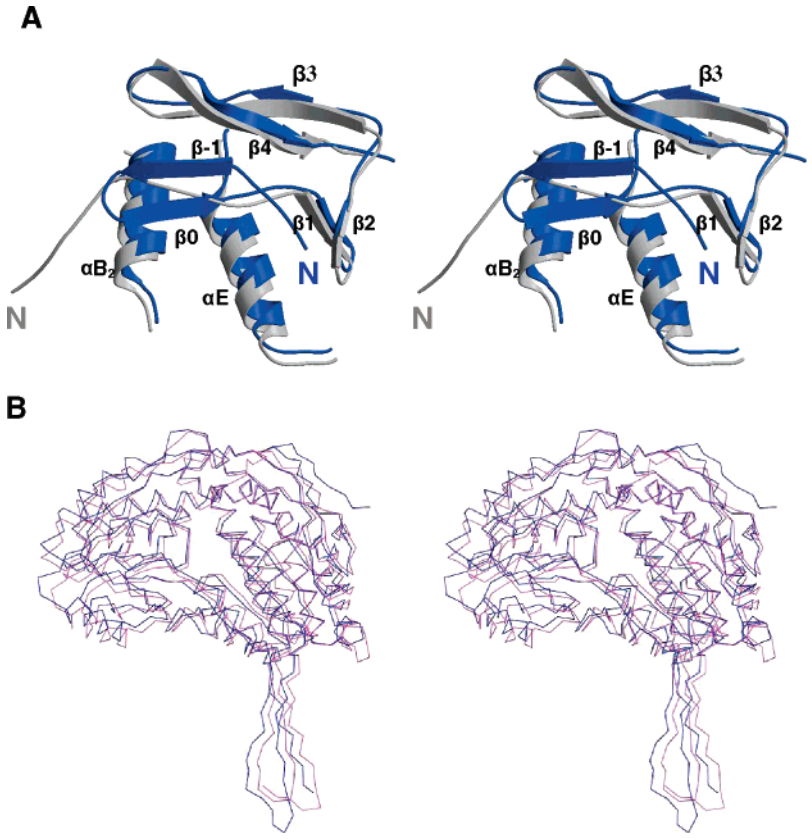

FIGURE 2: Comparison of the N-terminal region of C_t-FDH with human mitochondrial ALDH (PDB code 1O00). (A) In this stereoview, C_t-FDH in ribbon representation, which is colored blue, is superimposed onto human mitochondrial ALDH, which is colored gray. Secondary structure elements of C_t-FDH are labeled. (B) A stereoview of the superimposition of the overall folds of C_t-FDH (blue) vs human mitochondrial ALDH (magenta) in which both main chains are shown as C_α traces. The figure was prepared using MOLSCRIPT (*64*) and Raster3D (*65*).

refined with occupancy of 0.5 in all structures. We denote these two conformations of the sulfur atom as S^{Nat1} and S^{Nat2}. Two conformations of the equivalent cysteine were also observed in the structure of ALDH from *E. coli* (*31*).

Additional electron density next to the sulfhydryl group of Cys707 in the S^{Nat1} position suggests that this group may be oxidized. We have also detected similar modifications in several other structures of ALDH (see Supporting Information). It is well-established that the active site cysteine of glyceraldehyde 3-phosphate dehydrogenase can be oxidized to sulfenic, sulfinic, and sulfonic derivatives (*42*) and that such oxidation accompanies a loss of dehydrogenase activity and increase in acylphosphatase activity (*43*). The density suggests that a sulfenic derivative of Cys707 is present in C_t-FDH. This modification appears to be reversible because the same apo C_t-FDH crystals were used in soaking experiments to give the $NADP^+$-bound structure, which does not show a similar modification.

The side chain of Glu673 points directly toward Cys707, and its carboxylate oxygens are within 3.3 Å and 3.7 Å of S^{Nat1} and S^{Nat2}, respectively (Figure 3A). This close proximity between the glutamate and cysteine was also observed previously in the crystal structure of human ALDH2 (*25*) and is consistent with the role of Glu673 as a general base in deprotonation of Cys707 (in the absence of $NADP^+$), as suggested for human ALDH2 (*26*). The only other glutamate in this region, Glu804, whose equivalent has been suggested to be the thiol-activating general base in ALDH3 (*22*, *44*), is located 5.1 Å and 6.6 Å away from S^{Nat2} and S^{Nat1}, respectively (Figure 3A), and is unlikely to have any direct effect on catalysis in FDH.

E673A Mutant. To examine the role of Glu673 in catalysis, we mutated this residue to Ala in C_t-FDH and tested its ALDH activity using propanal as a substrate. In contrast to native C_t-FDH, no NADPH formation was detected at 340 nm, indicating an inactive enzyme (data not shown). However, if Cys707 could be activated without Glu673 (i.e., Glu673 is involved in deacylation only), as argued elsewhere (*21*, *27*), then the mutant enzyme should produce a burst of 1 mol of NADPH per 1 mol of C_t-FDH subunit before being blocked at the deacylation step. To test this, the concentration of the E673A mutant of C_t-FDH in the described assay was increased to 4.45 μM and the absorbance spectrum was recorded 2 min after addition of propanal. No corresponding formation of NAPDH could be detected under these conditions (Figure 4). These data are consistent with a major role for Glu673 in acylation.

$NADP^+$-Bound Structure. The structure of C_t-FDH in complex with $NADP^+$ was determined at 2.0 Å resolution. All C_α atoms of this structure could be superimposed onto those of native C_t-FDH with an rmsd of 0.23 Å, and there were no large-scale rearrangements of the protein structure due to binding of this cofactor in any of the four subunits. As in other ALDH enzymes (*22*, *23*), the coenzyme molecule is bound through a nonclassical Rossmann fold. The adenine part is bound in a cleft bordered by helices αF and αG with the β strands β7, β10, and β11 at the base (see Figure 1C). The pyrophosphate part of $NADP^+$ is relatively open to the

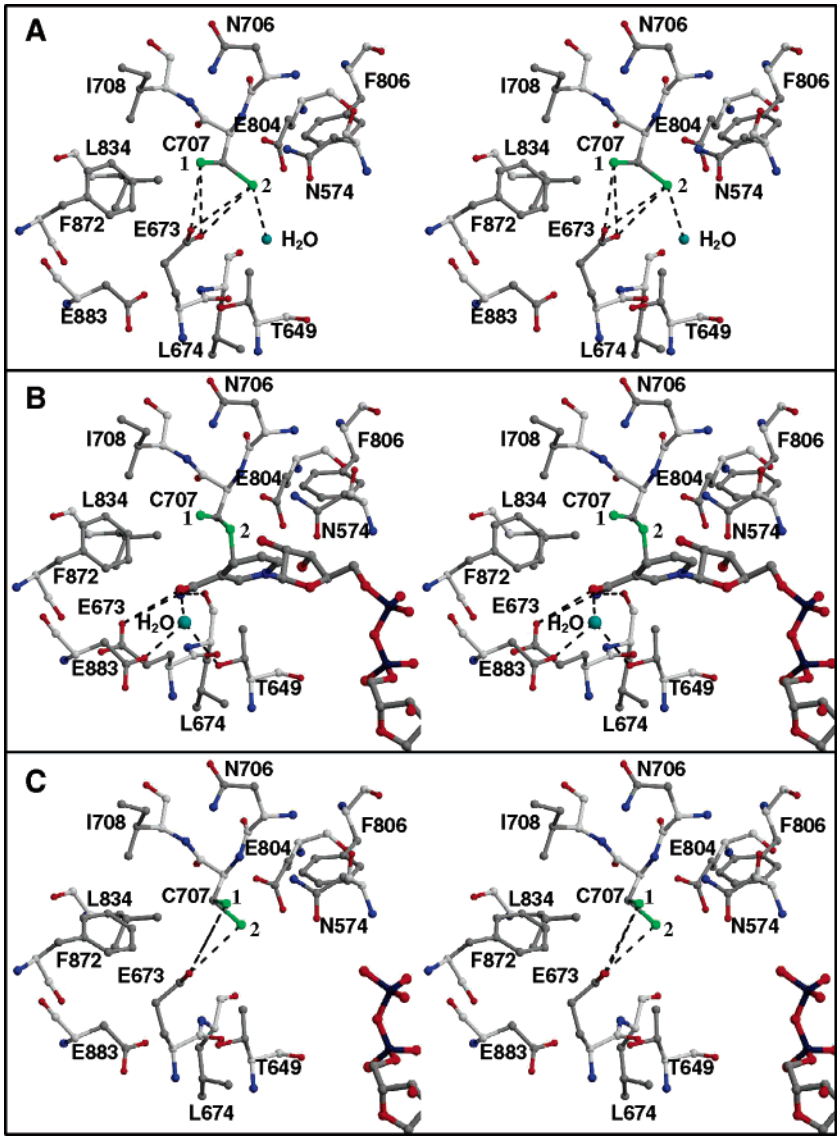

FIGURE 3: The active site region of the native, $NADP^+$-bound and NADPH-bound crystal structures of C_t-FDH. In these stereoviews, the two conformations of the sulfur atom of Cys707 are denoted as 1 (S^{Nat1}, S^{NADP1}, and S^{NADPH1}) and 2 (S^{Nat2}, S^{NADP2}, and S^{NADPH2}) and are colored green. Water molecules are shown as blue spheres. (A) The active site of the native protein. The potential hydrogen bonds involving the sulfur atom of Cys707 are shown as dashed lines. (B) The active site of the binary complex with $NADP^+$. The covalent link is shown between the sulfur atom of S^{NADP2} and the C4 atom of the nicotinamide ring. Selected hydrogen bonds involving the carboxyamide group of the nicotinamide ring are shown as dashed lines. (C) The active site of the binary complex with NADPH. The nicotinamide moiety of the coenzyme was disordered and is not shown. Potential hydrogen bonds of the sulfur atom of Cys707 are shown as dashed lines. The figure was prepared using MOLSCRIPT (*64*) and Raster3D (*65*).

solvent, while the ribose of the nicotinamide moiety and the nicotinamide ring itself are buried in a pocket that approaches the active site from a direction opposite to the substrate entrance tunnel. The electron density maps show a single well-defined conformation for the $NADP^+$ molecule with the nicotinamide moiety in the hydride transfer (or extended) conformation (see Supporting Information). Based on the electron density, a Mg^{2+} atom has been modeled into the structure between the oxygens of the adenine and nicotinamide phosphates of the pyrophosphate link, where it is commonly found in other ALDH enzymes (*32*).

The structure of C_t-FDH is significantly different from those of ALDH1 and 2 in the region where the protein contacts the 2′-phosphate group of NADP (Figure 5). An invariant Glu195 residue that forms a hydrogen bond with the 2′-hydroxyl oxygen of the adenine ribose of NAD in class 1 and 2 ALDH enzymes is substituted with Gln600 in C_t-FDH. Compared to Glu195, the side chain of Gln600 has moved away from the coenzyme (by apparent rotation around the C_β atom) to create the space necessary for the 2′-phosphate (Figure 5A). The side chain nitrogen of Gln600 forms a hydrogen bond with a tightly bound water molecule (*B*-factor 22.6 $Å^2$) that, in turn, is bound to a 2′-phosphate oxygen of NADP. Other notable differences in this region include a serine at position 629 compared to a Tyr224 (ALDH1) or Phe224 (ALDH2) and a valine at position 601 instead of a glutamine. Both of these changes, involving the replacement of larger groups with smaller ones, may help accommodate the altered position of Gln600.

The comparison with binding region for the 2′-phosphate group in NADP-specific ALDHs (*45*, *46*) is intriguing. Those enzymes have a threonine or serine residue in place of

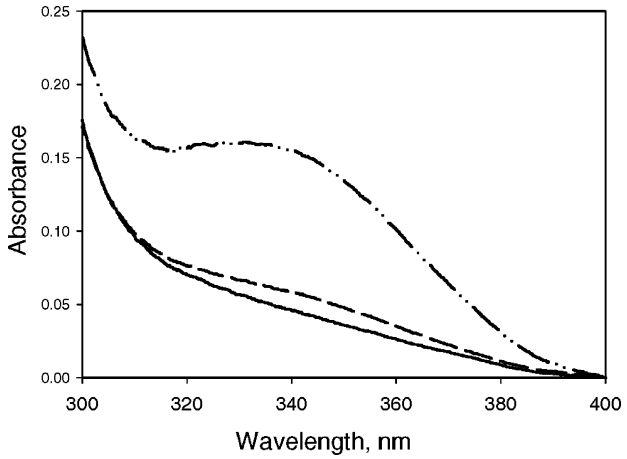

FIGURE 4: Verification of the role of Glu673 in acylation. Absorbance spectra of the Glu673Ala mutant of C_t-FDH in the reaction mixture before propanal was added (solid line) and 2 min after the addition of the substrate (dashed line). The protein concentration is 4.45 μM. The dash-and-dotted line represents the expected spectrum if the mutant enzyme was able to produce 1 mol of NADPH per 1 mol of protein subunit (the spectrum was obtained as a sum of the first curve and the spectrum of 17.8 μM NADPH). At this protein concentration, a residual level of aldehyde dehydrogenase activity could be detected after several hours of incubation (data not shown).

Gln600 in C_t-FDH (Figure 5C). At first sight, this would appear to be quite different from the binding mode observed in C_t-FDH, but, upon closer examination, the water molecule that bridges between the side chain of Gln600 and one of the 2′-phosphate oxygens overlaps quite closely with the hydroxyl group of the threonine (or serine) in NADP-specific ALDHs. Hence, in both cases, the phosphate is oriented by the same number and arrangement of hydrogen bonds, and it appears that the binding modes are in fact quite similar.

The major differences between the native and the $NADP^+$-bound structures are observed in the active site. In the $NADP^+$-bound structure, an apparent rotation about the $C_\alpha-C_\beta$ bond has moved the side chain of Glu673 away from Cys707 and the intervening space is now occupied by the nicotinamide ring (Figure 3B). In this structure, the side chain of Glu673 contacts a group of highly ordered water molecules located in a narrow channel that protrudes to the protein surface (Figure 6). The channel is situated at the intersubunit interface and is roughly perpendicular to the substrate entrance tunnel. The water molecules, together with carbonyls of Gly881 and Gly874, comprise a continuous chain of hydrogen bonding interactions and may represent a pathway for translocation of the proton abstracted by Glu673 from Cys707 to the solvent. A sulfate ion (from the mother liquor) is hydrogen bonded to two of the water molecules constituting the chain.

The nicotinamide ring of the cofactor is involved in several contacts with the protein (Figure 3B). Binding of $NADP^+$ induces a 180° flip of the carbonyl of Leu674 to become hydrogen-bonded to the carboxyamide nitrogen of the nicotinamide ring. This change in configuration was confirmed by $|F_O| - |F_C|$ electron density maps calculated after crystallographic refinements in which Leu674 and Gly675 were excluded from the model. Both atoms of the carboxyamide group of $NADP^+$ are within hydrogen-bonding distance of one of Glu673 side chain oxygens. In addition, the carboxyamide oxygen forms a hydrogen bond with a water molecule, which in turn is hydrogen-bonded to Asp883 and Thr649.

As in the native structure, two conformations are observed for the sulfur atom of Cys707, termed S^{NADP1} and S^{NADP2}, but, interestingly, one of these (S^{NADP2}) appears to be covalently linked to the C4 atom of the nicotinamide ring (Figure 3B). The existence of the covalent bond was confirmed by a series of crystallographic refinements that established the distance between the two atoms to be approximately 1.6 Å (Figure 7, see Supporting Information for details). Furthermore, the distorted nature of the electron density of the nicotinamide ring suggests a deviation from planarity that might be a result of the covalent bond to Cys707 due to the altered geometry at C4. This conclusion is also supported by the planarity of the same group in a 2.3 Å resolution crystal structure of a C707S mutant of C_t-FDH (data not shown). Additional evidence for a covalent adduct with $NADP^+$ came from absorption spectroscopy experiments: appearance of a peak at 300−340 nm was observed upon addition of $NADP^+$ to apo C_t-FDH (see Supporting Information).

Back soaking of a $NADP^+$-soaked crystal in mother liquor in the absence of coenzyme resulted in a crystal structure that showed no traces of the nicotinamide part of $NADP^+$ in the electron density, indicating that the covalent bond is reversible. Further evidence for the transient nature of the covalent bond comes from soaking experiments in the presence of $NADP^+$ (10 mM) and propanal (100 mM), either simultaneously or stepwise. These structures showed no substrate in the active site, while the electron density for the cofactor was identical to that of NADPH.

NADPH-Bound Structure. The structure of C_t-FDH in complex with NADPH was determined to 2.2 Å resolution. The protein fold of this structure shows a high degree of similarity to the $NADP^+$-bound structure with an rmsd of 0.14 Å between all C_α atoms. The major difference between the NADPH- and $NADP^+$-bound structures is in the respective positions of the nicotinamide moiety of the cofactor and the side chain of Glu673 (Figure 3C). As judged from the position of the nicotinamide phosphate, the reduced cofactor still occupies the hydride transfer (extended) conformation, but electron density corresponding to the nicotinamide ring of NADPH and the neighboring ribose is not visible (Figure S1B in Supporting Information), presumably due to disorder. This has also been observed in other ALDH enzymes (*30*). In the absence of the nicotinamide within the catalytic center, the side chain of Glu673 now occupies a position close to Cys707 in essentially the same manner as in the structure of the apoenzyme. The carbonyl of Leu674 is also the same as that of apo C_t-FDH, and two conformations are observed for Cys707 (though position 1 is slightly rotated with respect to that of the apoenzyme).

DISCUSSION

Coenzyme Specificity. Despite the high sequence and structural similarity with NAD-specific ALDH1 and ALDH2, C_t-FDH demonstrates a strong preference for NADP (*12*). To date, two structures of NADP-specific ALDH have been solved: GAPN from *Streptococcus mutans* (*45*) and ALDH from *Vibrio harvei* (*46*). In these structures, a threonine/

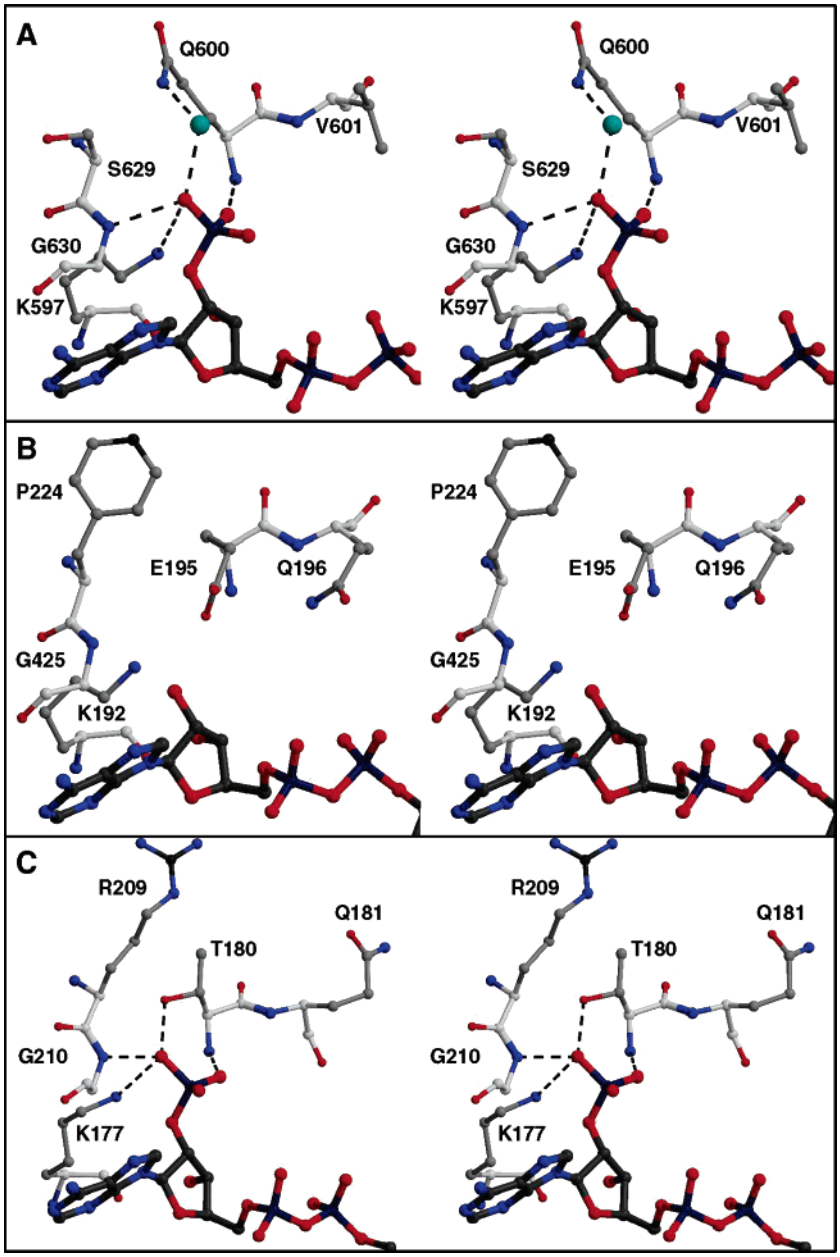

FIGURE 5: Molecular recognition of the 2′-phosphate of $NADP^+$ in Ct-FDH. (A) A stereoview of the 2′-phosphate binding region of $NADP^+$ in the crystal structure of C_t-FDH. All potential hydrogen bonding interactions between the enzyme and the phosphate are shown as dashed lines. Note how a water molecule (blue sphere) is positioned between the side chain amide nitrogen of Gln600 and a 2′-phosphate oxygen of $NADP^+$. (B) A stereoview of the equivalent region in the structure of human mitochondrial ALDH (PDB code 1O00), which is NAD specific. (C) A stereoview of the 2′-phosphate binding region of $NADP^+$ in the structure of GAPN from *S. mutans* (PDB code 2EUH). Although Gln600 of Ct-FDH is represented by Thr180 in this structure, note the overall similarity of the hydrogen bonding interactions involving the 2′-phosphate. In all structures, only the adenine part of the coenzyme is shown. The figure was prepared using MOLSCRIPT (*64*) and Raster3D (*65*).

serine (in place of Glu195 in ALDH1 and 2) helps orient the 2′-phosphate of NADP via its side chain hydroxyl as well as its main chain amide (Figure 5C). This led to the suggestion that a threonine or a serine at this position is unique for NADP-specific ALDH enzymes and is the primary determinant for coenzyme specificity (*45*, *46*). By containing Gln600 in place of a threonine/serine, C_t-FDH demonstrates a different mode for accommodating the 2′-phosphate. Despite this difference, though, the main chain amide contact with the phosphate is retained in C_t-FDH and, intriguingly, the hydroxyl-mediated contact of Thr/Ser is mimicked by a water molecule that bridges between the Gln side chain and the phosphate (Figure 5A). Hence, although it involves different amino acids, the mechanism of recognition at the physicochemical level is actually more similar than it initially appears and in evolutionary terms might be considered a convergent event.

Coenzyme Mobility. A hallmark of the ALDH family of enzymes is the unusual orientation of the NAD coenzyme within the Rossmann fold compared to other NAD-binding proteins (*22*, *23*). It has been suggested that the unusual binding mode of the coenzyme, in which the pyrophosphates form relatively weak contacts with the enzyme, permits the transition between the hydride transfer and hydrolysis positions of the nicotinamide ring during the reaction (*28*). In support of this, the hydride transfer position has been

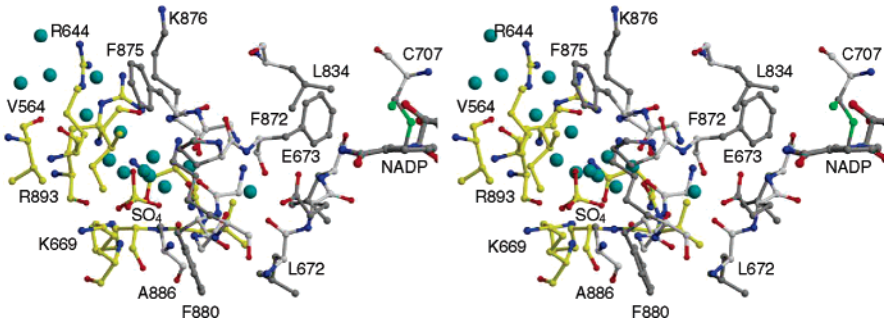

FIGURE 6: The putative proton translocation network of C_t-FDH. In this stereoview, water molecules are shown as blue spheres. The residues that belong to subunit A are colored gray; those that belong to subunit B are colored yellow. Only the nicotinamide ring of $NADP^+$ is shown. The figure was prepared using MOLSCRIPT (*64*) and Raster3D (*65*).

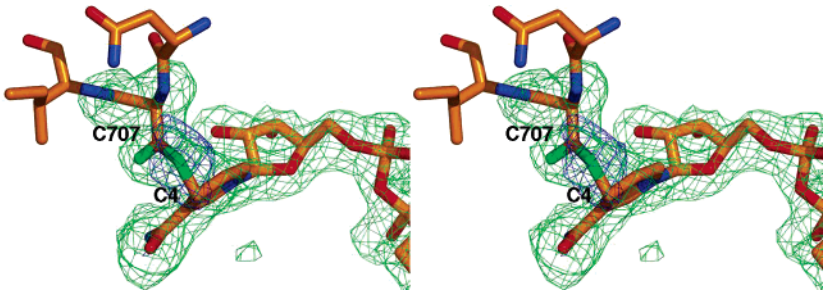

FIGURE 7: An apparent covalent bond between Cys707 and the nicotinamide ring in the crystal structure of C_t-FDH in complex with $NADP^+$. Stereoview of unbiased electron density that shows the covalent link between the S_γ atom of Cys707 and the C4 atom of $NADP^+$, set against the final model in which the length of the bond is 1.6 Å. Shown in green and contoured at 3 σ is the positive $|F_O| - |F_C|$ electron density map that was obtained after a refinement in which the occupancies of all atoms of Cys707 and $NADP^+$ were set to zero. Colored blue and contoured at 4 σ is the positive $|F_O| - |F_C|$ electron density map obtained after a refinement in which the occupancies of only S^{NADP2} and C4 atoms were set to zero. The figure was prepared using PyMOL (www.pymol.sourceforge.net).

observed in ALDH2 when oxidized coenzyme is bound and the hydrolysis position when the coenzyme is reduced (*32*). Flexibility of the coenzyme, correlated with enzymatic activity, has also been detected in ALDH2 using NMR and fluorescence spectroscopies (*47*). Our structures of C_t-FDH show a similar pattern. The nicotinamide moiety is well ordered when coenzyme occupies the hydride transfer position in the complex of C_t-FDH with $NADP^+$ but is apparently disordered in the complex with NADPH (we propose this to be analogous to the hydrolysis position). Similar disorder of the nicotinamide ring was also observed in the crystal structure of the YdcW ALDH from *E. coli* in complex with NADH (*31*), and in the structures of ALDH1 (*28*), ALDH2 (*23*), and GAPN from *Thermoproteus tenax* (*48*). Although these latter structures were complexes with $NAD(P)^+$, catalysis occurring within the crystals using trace aldehydes present in the crystallization solutions may have caused increased flexibility of the coenzyme as it became reduced (*32*). In fact, we observe this phenomenon directly in C_t-FDH because, when crystals of the enzyme in complex with $NADP^+$ are soaked in buffer containing an aldehyde substrate of FDH, propanal, the nicotinamide ring is not seen in the resulting structure, suggesting that it has become reduced and has shifted to the hydrolysis position (data not shown).

Concerted Motion of Glu673 and Coenzyme. The reaction catalyzed by ALDHs is believed to commence with binding of the oxidized coenzyme followed by the binding of substrate (*49*). Comparison of the three C_t-FDH structures presented here provides a snapshot of how the active site is rearranged as a result of coenzyme binding and how it is altered during the transition between oxidized and reduced forms of the coenzyme. Although binding of $NADP^+$ within the active site of C_t-FDH does not cause a significant rearrangement of the active site residues, the position of Glu673 is markedly different. In the structure of the apoenzyme, the carboxylate group of Glu673 is within hydrogen bonding distance of the sulfydryl of Cys707 whereas, in the complex with $NADP^+$, this side chain has rotated away from the cysteine and is now hydrogen bonded to the amide group of the nicotinamide. The C_t-FDH structure shows how the proton, abstracted by Glu673, can be released from the catalytic center to the milieu. A continuous network of water molecules and main chain carbonyl groups, all within hydrogen bonding distance of each other, leads from the side chain of the glutamate to the protein surface (Figure 6) and could be the path for removal of the proton. Such a proton shuttling network has also been seen in other enzymes; for example, carbonic anhydrase (*50*, *51*).

Interestingly, in the complex with NADPH, in which the nicotinamide moiety of the coenzyme is disordered and lies outside of the catalytic center, Glu673 occupies the same position as in the apo enzyme and the contact with Cys707 is restored. These structural data are consistent with the idea of a concerted motion of the glutamate and the nicotinamide occurring during catalysis, as has been suggested for ALDH1 (*28*). When $NADP^+$ binds, the nicotinamide occupies the hydride transfer position, which causes the displacement of the side chain of Glu673 away from the active center and thus breaks the contact between Cys707 and Glu673. When the coenzyme is reduced, however, the nicotinamide moves away from the active center, allowing Glu673 to rotate back in and restore its contact with Cys707. Most pertinently, these structures show that, prior to catalysis, in the absence of

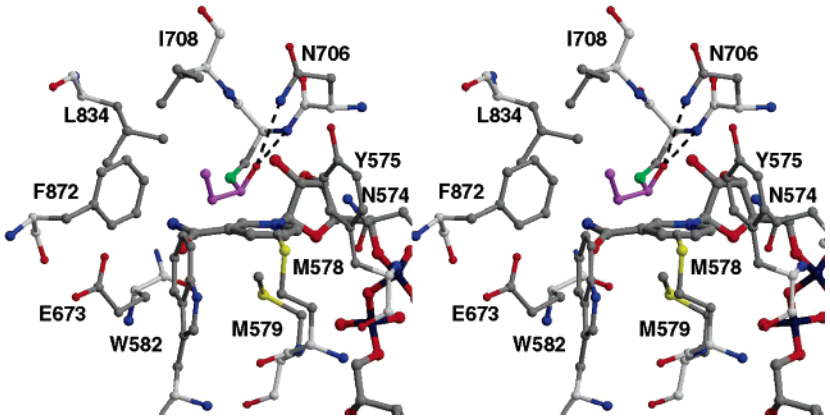

FIGURE 8: Modeling of aldehyde substrate into the active site of C_t-FDH. In this stereoview, a molecule of propanal (colored in magenta) is modeled into the active site of C_t-FDH, with bound $NADP^+$, as the thiohemiacetal intermediate. Dashed lines represent hydrogen bonds. The figure was prepared using MOLSCRIPT (*64*) and Raster3D (*65*).

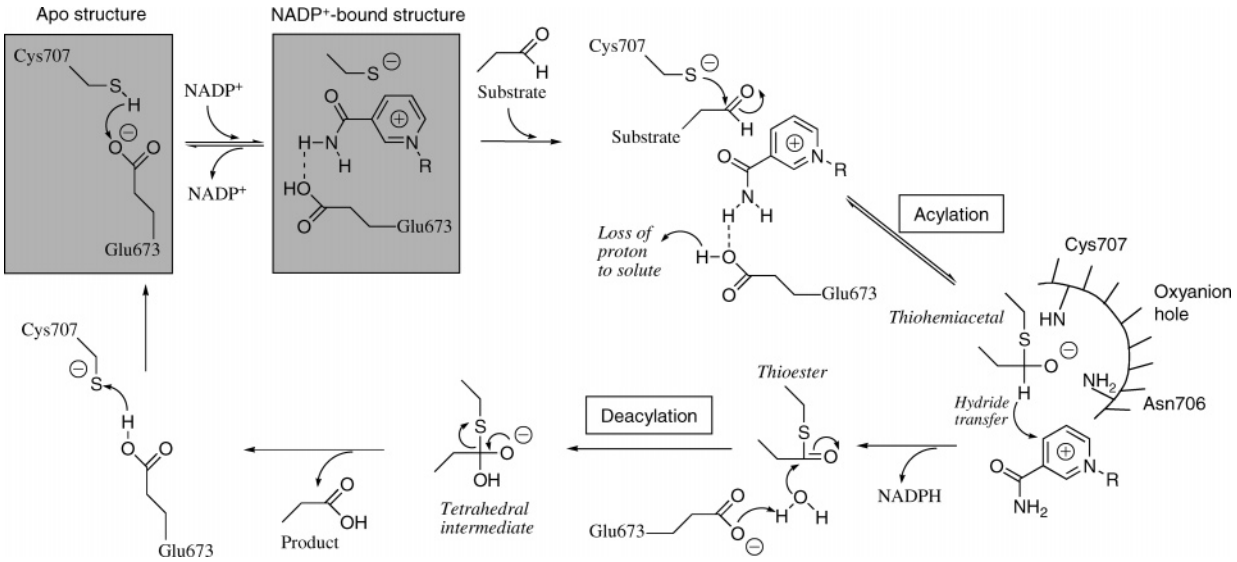

FIGURE 9: Proposed mechanism of the aldehyde dehydrogenase reaction catalyzed by FDH (see text for details). The gray boxes illustrate the arrangement of catalytic residues, Cys707 and Glu673, and the nicotinamide ring observed in the crystal structure of C_t-FDH in the apo and $NADP^+$-bound forms.

cofactor, Glu673 is well placed to abstract a proton from Cys707 and therefore probably plays a major role in acylation. This conclusion is supported by the mutation of Glu673 to an alanine, which results in a virtually inactive enzyme, including the absence of a burst of NADPH production at the onset of the reaction. A similar lack of NADH formation was observed in human ALDH2 when the equivalent Glu268 was substituted with glutamine, aspartate, and lysine (*26*). It should be taken into consideration, however, that our mutagenesis studies do not exclude the role of Glu673 in hydride transfer, where it may position the nicotinamide ring through the hydrogen bond with its carboxamide moiety. Overall, our structural, mutational, and spectroscopic studies support a major role of Glu673 in acylation in C_t-FDH, in contrast to other studies that have argued against the role of the glutamate in acylation (*27*, *52*). The restored close proximity of Glu673 to Cys707 when the coenzyme is in the hydrolysis position is also consistent with this residue playing a role in deacylation, which has been postulated previously (*23*, *27*, *28*).

Apparent Covalent Bond between Cys707 and Coenzyme. A series of crystallographic refinements indicates the presence of a covalent bond in C_t-FDH between one of the two conformations of the active site cysteine sulfur and the C4 atom of the nicotinamide ring of $NADP^+$. The deviation from planarity of the nicotinamide ring may be caused by partial tetrahedral geometry at C4. Furthermore, absorption spectroscopy indicated a small but measurable absorption band at around 320 nm after addition of $NADP^+$ to C_t-FDH (see Supporting Information), which is characteristic of adducts observed between NAD(P) and various sulfhydryl compounds (*53*). Similar interactions between nucleophilic groups and the nicotinamide ring of NAD/NADP have also been observed in other enzymes. In horse liver ADH, the N2 atom of pyrazole forms a partial covalent bond with C4 of NAD^+ (*54*). A covalent adduct detected in the structure of *Drosophila* ADH between C_α of 3-pentanone and the C4 atom of NAD^+ renders the enzyme inactive (*55*). A similar bond was observed between dihydroxyacetone phosphate and C4 of NAD^+ in GAPDH from *Leishmania mexicana* (*56*).

The presence of two apparent conformations for Cys707 (each modeled at 50% occupancy) in the complex of C_t-FDH with $NADP^+$ suggests that not all the $NADP^+$ molecules in the crystal are covalently bound to the cysteine. In the second position, the sulfur is 2.6 Å away from C4. We interpret this as equilibrium between two states: one

with a covalent linkage between C4 and the cysteine sulfur, and one with a longer range electrostatic interaction, with the positive charge at C4 and the negative charge on the sulfur (a sulfide anion).

An important issue raised by the covalent adduct is whether such a species is a part of the catalytic mechanism of C_t-FDH. Although it is difficult to envisage how the aldehyde substrate can react with the cysteine covalently bound to $NADP^+$, it could react with the thiolate of the dissociated state. A transient covalent bond might, therefore, help maintain the cysteine in an activated state after the side chain of Glu673 has been displaced from the active site or act as a holding mechanism for retention and correct orientation of the coenzyme in the hydride transfer position prior to substrate binding. On the other hand, the covalent adduct could simply represent an artifact that results from the nucleophilicity of the thiolate and the partial positive charge at C4 of $NADP^+$, which falls apart upon the substrate binding. Interestingly, we detected a similar covalent bond between Cys297 (the equivalent of Cys707 of C_t-FDH) and $NADP^+$ in the crystal structure of GAPN from *T. tenax* (*48*) (see Supporting Information). This suggests that similar covalent bonds may also occur in other members of the ALDH family. In this regard, "half-of-the-site" reactivity of some ALDH (*57*−*59*) could be explained in the context of a covalent bond between enzyme and coenzyme. Equilibrium between covalent and noncovalent states of $NADP^+$, each with approximately 50% occupancy, could result in only half of the active sites being active at a specific time point.

Overall Mechanism. To illustrate catalytic reaction of C_t-FDH, a propanal molecule covalently bound to Cys707 was modeled into the structure of the binary complex with $NADP^+$ (Figure 8). In this structure, the oxygen atom of the substrate is held by the side chain amide group of Asn706 and the main chain amide of Cys707. The rest of the substrate molecule is surrounded by essentially hydrophobic residues, such as Ile708, Leu834, Phe872, Trp582, Met578, and Met579.

Based on this model and our structural data, we propose a mechanism of catalysis in which Glu673 abstracts a proton from Cys707 to produce a thiolate and then, upon binding of $NADP^+$, is displaced and loses this proton to solvent via the network of ordered water molecules (Figure 9). After the binding of substrate, the thiolate attacks the carbonyl carbon of the aldehyde to form a thiohemiacetal intermediate. Transfer of the aldehyde hydride to C4 of the nicotinamide ring converts the thiohemiacetal to a thioester intermediate. At this stage, the reduced coenzyme leaves the active site (to become disordered or to occupy the hydrolysis position) and is replaced by a water molecule that is held in place by Glu673. The glutamate, now acting as a base for the second time, activates the water molecule for a nucleophilic attack at the carbonyl carbon, which, after passing through a tetrahedral intermediate, leads to product release. In the final step, Glu673 "back-donates" its proton, thus restoring the sulfhydryl group of Cys707. This mechanism is particularly attractive because the idea of a proton shuttle from Glu673 to the solvent resolves the apparent contradiction of how this residue can act as a base twice, once in acylation and again in deacylation.

Another noteworthy feature of this mechanism is that, because Glu673 formally abstracts a proton from Cys707 (as suggested by their close proximity in the apo structure), and subsequently moves away upon coenzyme binding, nucleophilic attack on the substrate produces an oxyanion in the thiohemiacetal intermediate rather than a hydroxyl. An oxyanion has also been proposed in the reaction scheme of other ALDH enzymes (*21*, *23*, *60*). An alternative view that derives from molecular modeling simulations in rat ALDH3 invokes a concerted proton transfer from the main chain amide of Cys243 to the carbonyl oxygen of the intermediate, resulting in a protonated thiohemiacetal (*61*). In C_t-FDH, however, formation of the oxyanion is considered more probable because this would dispense with the requirement for a base to abstract the proton from the thiohemiacetal upon transition to the thioester intermediate, which correlates with the absence of a suitable residue to perform this role. In the structure modeled with propanal, the nearest residue to the putative oxyanion is Asn706, which is unlikely to act as a base (Figure 8). Moreover, the side chain amide of Asn706 and main chain amide of Cys707 appear well placed to form an oxyanion hole that stabilizes the negative charge of the oxyanion. This environment for the substrate is distinctly different from that observed in GAPDH, the textbook example for catalysis of pyridine nucleotide-dependent aldehyde oxidation, where a histidine is believed to function as a base by abstracting the proton from the thiohemiacetal (*62*, *63*).

ACKNOWLEDGMENT

The authors would like to thank Dr. Ailsa Powell for technical assistance and Graham Solomons for helpful discussions. The X-ray crystallography facility used for this work is supported by the Medical University of South Carolina's Research Resource Facilities program. Data were also collected at Southeast Regional Collaborative Access Team (SER-CAT) 22-ID beamline at the Advanced Photon Source, Argonne National Laboratory.

SUPPORTING INFORMATION AVAILABLE

Description of (i) electron density for $NADP^+$ and NADPH complexed with C_t-FDH (Figure S1); (ii) possible chemical modification of the active site cysteine in ALDHs; (iii) verification of the presence of a covalent bond between Cys707 of C_t-FDH and the C4 atom of $NADP^+$; (iv) possible covalent bond in the structure of the allosteric nonphosphorylating GAPDH from *T. tenax*; and (v) evidence of the presence of a covalent bond in the structure of the binary complex with $NADP^+$ obtained by absorption spectroscopy. This material is available free of charge via the Internet at http://pubs.acs.org.

REFERENCES

1. Rios-Orlandi, E. M., Zarkadas, C. G., and MacKenzie, R. E. (1986) Formyltetrahydrofolate dehydrogenase-hydrolase from pig liver: simultaneous assay of the activities, *Biochim. Biophys. Acta 871*, 24−35.
2. Krupenko, S. A., and Oleinik, N. V. (2002) 10-formyltetrahydrofolate dehydrogenase, one of the major folate enzymes, is down-regulated in tumor tissues and possesses suppressor effects on cancer cells, *Cell. Growth Differ. 13*, 227−236.
3. Oleinik, N. V., Krupenko, N. I., Priest, D. G., and Krupenko, S. A. (2005) Cancer cells activate p53 in response to 10-formyltetrahydrofolate dehydrogenase expression, *Biochem. J. 391*, 503−511.

4. Oleinik, N. V., and Krupenko, S. A. (2003) Ectopic expression of 10-formyltetrahydrofolate dehydrogenase in a549 cells induces g(1) cell cycle arrest and apoptosis, *Mol. Cancer Res. 1*, 577−588.
5. Krebs, H. A., Hems, R., and Tyler, B. (1976) The regulation of folate and methionine metabolism, *Biochem. J. 158*, 341−353.
6. Cook, R. J., and Wagner, C. (1982) Purification and partial characterization of rat liver folate binding protein: cytosol I, *Biochemistry 21*, 4427−4434.
7. Min, H., Shane, B., and Stokstad, E. L. (1988) Identification of 10-formyltetrahydrofolate dehydrogenase-hydrolase as a major folate binding protein in liver cytosol, *Biochim. Biophys. Acta 967*, 348−353.
8. Tephly, T. R. (1991) The toxicity of methanol, *Life Sci. 48*, 1031−1041.
9. Cook, R. J., Champion, K. M., and Giometti, C. S. (2001) Methanol toxicity and formate oxidation in NEUT2 mice, *Arch. Biochem. Biophys. 393*, 192−198.
10. Anguera, M. C., Field, M. S., Perry, C., Ghandour, H., Chiang, E. P., Selhub, J., Shane, B., and Stover, P. J. (2006) Regulation of Folate-mediated One-carbon Metabolism by 10-Formyltetrahydrofolate Dehydrogenase, *J. Biol. Chem. 281*, 18335−18342.
11. Cook, R. J., Lloyd, R. S., and Wagner, C. (1991) Isolation and characterization of cDNA clones for rat liver 10-formyltetrahydrofolate dehydrogenase, *J. Biol. Chem. 266*, 4965−4973.
12. Krupenko, S. A., Wagner, C., and Cook, R. J. (1997) Expression, purification, and properties of the aldehyde dehydrogenase homologous carboxyl-terminal domain of rat 10-formyltetrahydrofolate dehydrogenase, *J. Biol. Chem. 272*, 10266−10272.
13. Krupenko, S. A., Wagner, C., and Cook, R. J. (1997) Domain structure of rat 10-formyltetrahydrofolate dehydrogenase, Resolution of the amino-terminal domain as 10-formyltetrahydrofolate hydrolase, *J. Biol. Chem. 272*, 10273−10278.
14. Chumanevich, A. A., Krupenko, S. A., and Davies, C. (2004) The crystal structure of the hydrolase domain of 10-formyltetrahydrofolate dehydrogenase: mechanism of hydrolysis and its interplay with the dehydrogenase domain, *J. Biol. Chem. 279*, 14355−14364.
15. Reuland, S. N., Vlasov, A. P., and Krupenko, S. A. (2003) Disruption of a calmodulin central helix-like region of 10-formyltetrahydrofolate dehydrogenase impairs its dehydrogenase activity by uncoupling the functional domains, *J. Biol. Chem. 278*, 22894−22900.
16. Reuland, S. N., Vlasov, A. P., and Krupenko, S. A. (2006) Modular organization of FDH: Exploring the basis of hydrolase catalysis, *Protein Sci. 15*, 1076−1084.
17. Perozich, J., Nicholas, H., Wang, B. C., Lindahl, R., and Hempel, J. (1999) Relationships within the aldehyde dehydrogenase extended family, *Protein Sci. 8*, 137−146.
18. Schirch, D., Villar, E., Maras, B., Barra, D., and Schirch, V. (1994) Domain structure and function of 10-formyltetrahydrofolate dehydrogenase, *J. Biol. Chem. 269*, 24728−24735.
19. Feldman, R. I., and Weiner, H. (1972) Horse liver aldehyde dehydrogenase. II. Kinetics and mechanistic implications of the dehydrogenase and esterase activity, *J. Biol. Chem. 247*, 267−272.
20. Sheikh, S., Ni, L., Hurley, T. D., and Weiner, H. (1997) The potential roles of the conserved amino acids in human liver mitochondrial aldehyde dehydrogenase, *J. Biol. Chem. 272*, 18817−18822.
21. Marchal, S., Cobessi, D., Rahuel-Clermont, S., Tete-Favier, F., Aubry, A., and Branlant, G. (2001) Chemical mechanism and substrate binding sites of NADP-dependent aldehyde dehydrogenase from Streptococcus mutans, *Chem. Biol. Interact. 130-132*, 15−28.
22. Liu, Z. J., Sun, Y. J., Rose, J., Chung, Y. J., Hsiao, C. D., Chang, W. R., Kuo, I., Perozich, J., Lindahl, R., Hempel, J., and Wang, B. C. (1997) The first structure of an aldehyde dehydrogenase reveals novel interactions between NAD and the Rossmann fold, *Nat. Struct. Biol. 4*, 317−326.
23. Steinmetz, C. G., Xie, P., Weiner, H., and Hurley, T. D. (1997) Structure of mitochondrial aldehyde dehydrogenase: the genetic component of ethanol aversion, *Structure 5*, 701−711.
24. Lamb, A. L., and Newcomer, M. E. (1999) The structure of retinal dehydrogenase type II at 2.7 A resolution: implications for retinal specificity, *Biochemistry 38*, 6003−6011.
25. Hurley, T. D., Perez-Miller, S., and Breen, H. (2001) Order and disorder in mitochondrial aldehyde dehydrogenase, *Chem. Biol. Interact. 130-132*, 3−14.
26. Wang, X., and Weiner, H. (1995) Involvement of glutamate 268 in the active site of human liver mitochondrial (class 2) aldehyde dehydrogenase as probed by site-directed mutagenesis, *Biochemistry 34*, 237−243.
27. Marchal, S., Rahuel-Clermont, S., and Branlant, G. (2000) Role of glutamate-268 in the catalytic mechanism of nonphosphorylating glyceraldehyde-3-phosphate dehydrogenase from Streptococcus mutans, *Biochemistry 39*, 3327−3335.
28. Moore, S. A., Baker, H. M., Blythe, T. J., Kitson, K. E., Kitson, T. M., and Baker, E. N. (1998) Sheep liver cytosolic aldehyde dehydrogenase: the structure reveals the basis for the retinal specificity of class 1 aldehyde dehydrogenases, *Structure 6*, 1541−1551.
29. Johansson, K., El-Ahmad, M., Ramaswamy, S., Hjelmqvist, L., Jornvall, H., and Eklund, H. (1998) Structure of betaine aldehyde dehydrogenase at 2.1 A resolution, *Protein Sci. 7*, 2106−2117.
30. Cobessi, D., Tete-Favier, F., Marchal, S., Branlant, G., and Aubry, A. (2000) Structural and biochemical investigations of the catalytic mechanism of an NADP-dependent aldehyde dehydrogenase from Streptococcus mutans, *J. Mol. Biol. 300*, 141−152.
31. Gruez, A., Roig-Zamboni, V., Grisel, S., Salomoni, A., Valencia, C., Campanacci, V., Tegoni, M., and Cambillau, C. (2004) Crystal structure and kinetics identify Escherichia coli YdcW gene product as a medium-chain aldehyde dehydrogenase, *J. Mol. Biol. 343*, 29−41.
32. Perez-Miller, S. J., and Hurley, T. D. (2003) Coenzyme isomerization is integral to catalysis in aldehyde dehydrogenase, *Biochemistry 42*, 7100−7109.
33. Krupenko, S. A., and Wagner, C. (1998) Overexpression of functional hydrolase domain of rat liver 10-formyltetrahydrofolate dehydrogenase in Escherichia coli, *Protein Expr. Purif. 14*, 146−152.
34. Matthews, B. W. (1968) Solvent content of protein crystals, *J. Mol. Biol. 33*, 491−497.
35. Otwinowski, Z., and Minor, W. (1997) Processing of X-ray diffraction data collected in oscillation mode, *Methods Enzymol. 276*, 307−326.
36. Vagin, A., Teplyakov, A. (1997) MOLREP: an automated program for molecular replacement, *J. Appl. Crystallogr. 30*, 1022−1025.
37. Brunger, A. T., Adams, P. D., Clore, G. M., DeLano, W. L., Gros, P., Grosse-Kunstleve, R. W., Jiang, J. S., Kuszewski, J., Nilges, M., Pannu, N. S., Read, R. J., Rice, L. M., Simonson, T., and Warren, G. L. (1998) Crystallography & NMR system: A new software suite for macromolecular structure determination, *Acta Crystallogr. D Biol. Crystallogr. 54*, 905−921.
38. Murshudov, G. N., Vagin, A. A., and Dodson, E. J. (1997) Refinement of macromolecular structures by the maximum-likelihood method, *Acta Crystallogr. D Biol. Crystallogr. 53*, 240−255.
39. Jones, T. A., Zou, J. Y., Cowan, S. W., and Kjeldgaard. (1991) Improved methods for building protein models in electron density maps and the location of errors in these models, *Acta Crystallogr. A 47* (Part 2), 110−119.
40. Perrakis, A., Harkiolaki, M., Wilson, K. S., and Lamzin, V. S. (2001) ARP/wARP and molecular replacement, *Acta Crystallogr. D Biol. Crystallogr. 57*, 1445−1450.
41. Laskowski, R. A., MacArthur, M. W., Moss, D. S., Thornton, J. M. (1993) PROCHECK: a program to check the stereochemical quality of protein structures, *J. Appl. Crystallogr. 26*, 283−291.
42. Little, C., and O'Brien, P. J. (1969) Mechanism of peroxide-inactivation of the sulphydryl enzyme glyceraldehyde-3-phosphate dehydrogenase, *Eur. J. Biochem. 10*, 533−538.
43. Schmalhausen, E. V., Nagradova, N. K., Boschi-Muller, S., Branlant, G., and Muronetz, V. I. (1999) Mildly oxidized GAPDH: the coupling of the dehydrogenase and acyl phosphatase activities, *FEBS Lett. 452*, 219−22.
44. Wymore, T., Hempel, J., Cho, S. S., Mackerell, A. D., Jr., Nicholas, H. B., Jr., and Deerfield, D. W., 2nd. (2004) Molecular recognition of aldehydes by aldehyde dehydrogenase and mechanism of nucleophile activation, *Proteins 57*, 758−771.
45. Cobessi, D., Tete-Favier, F., Marchal, S., Azza, S., Branlant, G., and Aubry, A. (1999) Apo and holo crystal structures of an NADP-dependent aldehyde dehydrogenase from Streptococcus mutans, *J. Mol. Biol. 290*, 161−173.
46. Ahvazi, B., Coulombe, R., Delarge, M., Vedadi, M., Zhang, L., Meighen, E., and Vrielink, A. (2000) Crystal structure of the NADP+-dependent aldehyde dehydrogenase from Vibrio harveyi: structural implications for cofactor specificity and affinity, *Biochem. J. 349* (Part 3), 853−861.

47. Hammen, P. K., Allali-Hassani, A., Hallenga, K., Hurley, T. D., and Weiner, H. (2002) Multiple conformations of NAD and NADH when bound to human cytosolic and mitochondrial aldehyde dehydrogenase, *Biochemistry 41*, 7156−7168.
48. Pohl, E., Brunner, N., Wilmanns, M., and Hensel, R. (2002) The crystal structure of the allosteric non-phosphorylating glyceraldehyde-3-phosphate dehydrogenase from the hyperthermophilic archaeum Thermoproteus tenax, *J. Biol. Chem. 277*, 19938−19945.
49. Duncan, R. J. (1985) Aldehyde dehydrogenase. An enzyme with two distinct catalytic activities at a single type of active site, *Biochem. J. 230*, 261−267.
50. Jude, K. M., Wright, S. K., Tu, C., Silverman, D. N., Viola, R. E., and Christianson, D. W. (2002) Crystal structure of F65A/Y131C-methylimidazole carbonic anhydrase V reveals architectural features of an engineered proton shuttle, *Biochemistry 41*, 2485−2491.
51. Bhatt, D., Tu, C., Fisher, S. Z., Hernandez Prada, J. A., McKenna, R., and Silverman, D. N. (2005) Proton transfer in a Thr200His mutant of human carbonic anhydrase II, *Proteins 61*, 239−245.
52. Marchal, S., and Branlant, G. (1999) Evidence for the chemical activation of essential cys-302 upon cofactor binding to nonphosphorylating glyceraldehyde 3-phosphate dehydrogenase from Streptococcus mutans, *Biochemistry 38*, 12950−12958.
53. Van Eys, J., and Kaplan, N. O. (1957) The addition of sulfhydryl compounds to diphosphopyridine nucleotide and its analogues, *J. Biol. Chem. 228*, 305−314.
54. Rubach, J. K., and Plapp, B. V. (2003) Amino acid residues in the nicotinamide binding site contribute to catalysis by horse liver alcohol dehydrogenase, *Biochemistry 42*, 2907−2915.
55. Benach, J., Atrian, S., Gonzalez-Duarte, R., and Ladenstein, R. (1999) The catalytic reaction and inhibition mechanism of Drosophila alcohol dehydrogenase: observation of an enzyme-bound NAD-ketone adduct at 1.4 Å resolution by X-ray crystallography, *J. Mol. Biol. 289*, 335−355.
56. Choe, J., Guerra, D., Michels, P. A., and Hol, W. G. (2003) Leishmania mexicana glycerol-3-phosphate dehydrogenase showed conformational changes upon binding a bi-substrate adduct, *J. Mol. Biol. 329*, 335−349.
57. Weiner, H., Hu, J. H., and Sanny, C. G. (1976) Rate-limiting steps for the esterase and dehydrogenase reaction catalyzed by horse liver aldehyde dehydrogenase, *J. Biol. Chem. 251*, 3853−3855.
58. Zhou, J., and Weiner, H. (2000) Basis for half-of-the-site reactivity and the dominance of the K487 oriental subunit over the E487 subunit in heterotetrameric human liver mitochondrial aldehyde dehydrogenase, *Biochemistry 39*, 12019−12024.
59. Weiner, H., Wei, B., and Zhou, J. (2001) Subunit communication in tetrameric class 2 human liver aldehyde dehydrogenase as the basis for half-of-the-site reactivity and the dominance of the oriental subunit in a heterotetramer, *Chem. Biol. Interact. 130-132*, 47−56.
60. D'Ambrosio, K., Pailot, A., Talfournier, F., Didierjean, C., Benedetti, E., Aubry, A., Branlant, G., and Corbier, C. (2006) The first crystal structure of a thioacylenzyme intermediate in the ALDH family: new coenzyme conformation and relevance to catalysis, *Biochemistry 45*, 2978−2986.
61. Wymore, T., Deerfield, D. W., 2nd, Field, M. J., Hempel, J., and Nicholas, H. B., Jr. (2003) Initial catalytic events in class 3 aldehyde dehydrogenase: MM and QM/MM simulations, *Chem. Biol. Interact. 143-144*, 75−84.
62. Skarzynski, T., Moody, P. C., and Wonacott, A. J. (1987) Structure of holo-glyceraldehyde-3-phosphate dehydrogenase from Bacillus stearothermophilus at 1.8 Å resolution, *J. Mol. Biol. 193*, 171−187.
63. Soukri, A., Mougin, A., Corbier, C., Wonacott, A., Branlant, C., and Branlant, G. (1989) Role of the histidine 176 residue in glyceraldehyde-3-phosphate dehydrogenase as probed by site-directed mutagenesis, *Biochemistry 28*, 2586−2592.
64. Kraulis, P. J. (1991) MOLSCRIPT: a program to produce both detailed and schematic plots of protein structures, *J. Appl. Crystallogr. 24*, 946−950.
65. Merritt, E. A., Bacon, D. J. (1997) Raster3D: photorealistic molecular graphics, *Methods Enzymol. 277*, 505−524.

BI0619573